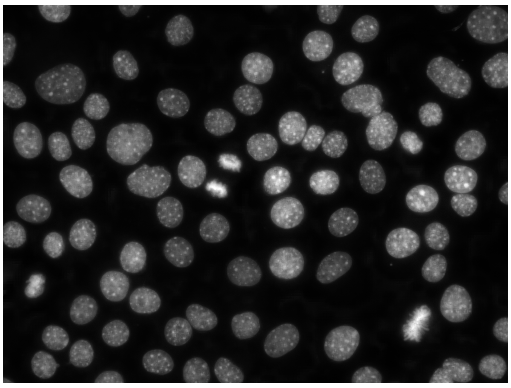

Deep Learning Techniques for Cell Stage Classification

Rafael José Costa Freitas

Thesis to obtain the Master of Science Degree in

Aerospace Engineering

Supervisor(s): Prof. Luis Custódio
Prof. João Sanches

Examination Committee

Chairperson: Prof. Jose Fernando Alves da Silva
Supervisor: Prof. Jõao Sanches
Member of the Committee: Prof. Margarida Silveira

October 2020

Dedicated to my friends and family who never allowed me to forget I was still not a master...

Acknowledgments

First, I would like to thank my thesis supervisors, Luis Custódio and João Sanches, for all their help and support. While it became a long journey to finalize this master thesis, their support and valuable counseling definitely provided me with all I needed to perform this work.

Next, I would like to thank my family, their unconditional support and love has encouraged me along my entire journey as a student and has shaped me into the person I am today. You are always there for me and there is no possible way I could thank you enough. I would also like to take this opportunity to apologize for all headaches and concerns I caused along the years, even though I cannot promise I will not do it again.

Next there are my friends. You have helped me every step of the way, from working on the various projects we had through college, to always giving me valuable advice or to, probably most important of all, providing me with the required fun moments and memories to really appreciate these years.

Resumo

O ciclo celular corresponde aos vários processos e mecanismos que ocorrem durante as diversas fases da vida de uma célula e a progressão correta ao longo do mesmo é essencial para a manutenção da vida.

Para uma célula eucariótica típica, este ciclo pode ser separado em 2 fases principais: a interfase, durante a qual a célula está em crescimento, e a mitose, onde a célula se separa em duas células filhas. A interfase pode ainda ser dividida em 3 fases principais, G1, onde a célula está em fase de crescimento, a fase S, onde o DNA celular é replicado e a fase G2, durante a qual a célula continua a preparação para a mitose.

Devido à importância do ciclo celular, a classificação correta da fase celular é essencial para a pesquisa biológica e farmacológica. Porém, os métodos atuais de classificação celular baseiam-se tradicionalmente na microscopia fluorescente e em análises populacionais. Assim sendo, estes métodos apresentam algumas desvantagens, como a necessidade de marcadores biológicos específicos ou a destruição da cultura celular para determinar a fase celular.

Como tal, neste projecto é proposto um novo método que se baseia no uso de culturas de células marcadas com o composto DAPI (uma das técnicas de microscopia fluorescente mais comuns) e técnicas de deep learning. Utilizando algoritmos de deep learning, este método é capaz de classificar células isoladamente sem depender de análises populacionais e sem necessitar de marcadores biológicos específicos, resultando num processo bastante mais simples para classificar a fase celular.

Palavras-chave: *Deep Learning*, Composto DAPI, Microscopia Fluorescente, Ciclo Celular, Rede Neuronal Convolucional

Abstract

The various phases and mechanisms that happen sequentially during a life of a cell form the cell cycle and the correct progression along this cycle is essential for the maintenance of life.

For a typical eukaryotes cell this cycle can be separated into 2 main phases: interphase, during which the cell is growing, and mitosis, where the cell separates into two daughter cells. The interphase can be further divided into 3 main phases, G1, where the cell is growing, the S phase, where the DNA is replicated and the G2 phase during which the cell continues growing in preparation for mitosis.

Due to the importance of the cellular cycle, the correct staging of a cell (i.e. correct classification of its current phase) is of the utmost importance for biological and pharmacological research. However, current methods for cell staging have traditionally relied on fluorescence microscopy and the analysis of cell population and present some drawbacks such as the need for specific biological markers or the destruction of the cell culture to determine its stage.

As such, in this project, a new method that relies on the use of DAPI stained cell cultures (one of the most common cell imaging techniques) and deep learning techniques is proposed. By using deep learning algorithms, this method is capable of classifying single data points without relying on cell population analysis and will not require specific biological markers, resulting in fairly simpler process to achieve cell staging.

Keywords: Deep learning, DAPI staining, Fluorescent Microscopy, Cell Cycle, Convolutional Neural Network

Contents

List of Tables

List of Figures

Glossary

ANN	Artificial Neural Network
CNN	Convolutional Neural Network.
DAPI	40,60-Diamidino-2-Phenylindole, Dihydrochloride.
AT	Adenine and thymine, a base pair in DNA.
DNA	Deoxyribonucleic acid.
FM	Fluorescent Microscopy.
FUCCI	Fluorescent Ubiquitination-based Cell Cycle Indicator.
ML	Machine learning.
MNIST	Modified National Institute of Standards and Technology.
RNA	Ribonucleic acid.

Chapter 1

Introduction

1.1 Motivation

The cell cycle is one of the essential mechanisms that allow the maintenance of life. The correct progression along the cell cycle makes cell growth and reproduction possible by achieving its separation into two daughter cells with equal genome.

Across the cell cycle, genome stability is maintained by regulatory mechanisms that ensure not only the correct genome duplication, but also the appropriate chromosomal distribution to each daughter cell. Failure of these mechanisms may cause genome instability which has been linked to abnormal cellular behavior, such as unscheduled proliferation, and to diseases, one such example being cancer. [1, 2]

As such, the study of cell cycle progression is of the utmost importance for biological and pharmaceutical research, as is the ability to determine at which stage a cell is, i.e., the ability to stage a cell. Most cell staging methods rely on population-based analysis making them incompatible with single-cell staging.

Traditionally, the cell cycle phase is monitored through the use of cell markers such as the FUCCI compound used during this work. Paired with fluorescence microscopy, these markers are capable of displaying the progression of a cell along the cellular cycle.

However, most of these markers present limitations such as only being capable of manifesting one specific cell stage or being incompatible with modern high-resolution biological techniques. [3–5]As such, a less invasive and more simpler approach to cellular classification would be useful for many types of biological and clinical tests. For example, it would be useful to monitor the localization and organization of certain cellular components along the cell cycle.[6]

Recent work has been developed to use machine learning methods to stage cells based on their biological features, such as organelle positioning, size of nucleus and amount of DNA, and not relying on biological markers. The use of deep learning techniques could result in methods capable of classifying the cellular stage while being compatible with other modern biological techniques. [7]

1.2 Objectives

This work aims to evaluate cells through 40,60-diamidino-2-phenylinodole (DAPI) staining with fluorescence microscopy images and classify them by identifying the corresponding cell cycle phase, considering intracellular features. While some approaches have relied on the clustering classification and could only classify accurately a sufficiently large set of data points, this can be problematic due to the complexity and low throughput of current imaging techniques. Additionally, there is the need for classification of singular data points in biological investigation, which cannot be performed with cluster classification. By using deep learning methods, this work aims to develop a method that can successfully identify single data points after careful training is performed with the original dataset.

1.3 Thesis Outline

The first chapter of this thesis will shed light the motivation and objectives pursued along the development of this work. The second chapter of this thesis will provide the theoretical background required, both in the eukaryotic cell cycle and in machine learning basics. Initially this section will describe cell evolution across the cell cycle and the different mechanisms that occur to ensure the correct and successful progression along this cycle. Secondly, a brief overview of current cell imaging and staging techniques will be provided to better understand how to interpret the biological data that was the basis for this work. Finally, this section will also give a brief theoretical explanation on the machine learning concepts used to develop the different classification algorithms. The third chapter of this thesis will provide an explanation on how the theoretical concepts previously explained will be explored in this master thesis, including an explanation on how the biological data was used to produce the required information to train and develop the deep learning algorithms utilized. Finally, the forth chapter will present the results obtained during the development of this work and the fifth and final chapter will provide a brief discussion on the results obtained.

Chapter 2

Theoretical Background

This chapter will present a brief summary of the necessary theoretical concepts. Since the thesis has a biological component and a computational component, the chapter is divided in two parts, each explaining the biological concepts and the computational concepts.

2.1 Biological Background

2.1.1 The Cell

Cells are the basic unit of life and are considered the building blocks of all living organisms. Much like these organisms, cells have evolved and adapted to various environments and functional roles. Nonetheless, all cells basically rely on the same structures (illustrated in figure 2.1) to perform the set of tasks essential for their own survival. In fact, these similarities are what defines a cell. [8]

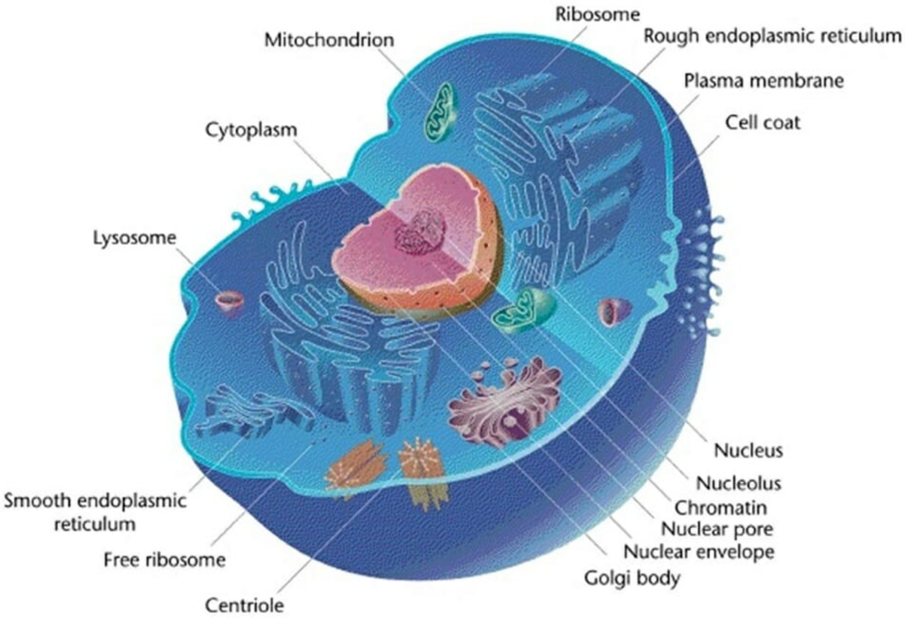

Figure 2.1: Diagram of eukaryotic cell. Source: [9]

The cell membrane, or plasma membrane, is one of these common structures. Formed by a semipermeable, phospholipidic dual layer, this structure encapsulates the entire cell and is responsible for regulating the cells interactions with its environment. On a cellular scale, these interactions are translated in the emission and absorption of certain molecules. As such, the main function of the plasma membrane is to act as a gatekeeper and determine which molecules can cross the membrane and which cannot. To this end, the membrane is studded with proteins that perform this function, amongst others. On the inside of this membrane, the cytoplasm, a water based liquid environment, constitutes the interior of the cell.

Another one of these common aspects is that all cells possess nucleic acids (the molecules responsible for containing and helping to express a cell's genetic code [8]). These acids can be classified in two major classes deoxyribonucleic acid (DNA), that contains the essential information for the creation and maintenance of the cell and ribonucleic acid (RNA), that possesses several roles associated with the expression of genetic material. The DNA is packaged differently in different cells which resulted in a form of cell classification, if the DNA presents itself separated from the cytoplasm by an envelope, then the cell is eukaryote. In contrast, if the DNA is in contact with the cytoplasm, without any barrier, then the cell is prokaryote. Eukaryotic cells form all animals and plants. As such, since the data used on this thesis refers to human cells, these will be the ones of interest. Consequently, every time the term cell is used, it is in reference to eukaryotic cells.

Every eukaryotic cell (from here onward just referred to as cell) possesses a nucleus, a structure that stores the cells' DNA. This structure is separated from the cytoplasm by a membrane that allows the passage of proteins into the nucleus and the passage of ribosomal subunits out of the nucleus. This structure is of substantial importance since it stores the genetic information that contains the cell's function and characteristics. Even though, all cells possess the same genetic information, only a few genes are expressed according to the cell function.[8]

Cells also possess proteins in their cytoplasm: These chains of amino acids serve a variety of functions in a cell, such as catalytic or structural. Cells also possess organelles. These partitioned structures perform specific functions essential for the correct functioning of the cell. One such example is a mitochondrion, responsible for the energy production for the entire cell. [8]

2.1.2 The Cell Cycle

As most living beings, cells possess a life cycle. This life cycle, or the cell cycle, describes all the processes that a cell goes through to replicate its components, particularly its genome, to successfully divide into two daughter cells. [10]

Clearly, the cell cycle includes an orderly sequence of events to achieve this end and can be divided into four phases: gap 1 (G1), synthesis (S), gap 2 (G2) and M phase (which comprises the mitosis and the cytokinesis), which occur in this order. A fifth state exists, named G0. This state corresponds to a non-dividing stage and, is a branch of the G1 phase. [11] Each of the stages possess a specific role and the entire process is controlled by a set of enzymes, the cyclin dependent kinases (CDK's). As the name sugests, these enzymes are regulated by cyclins, a protein group that appears and disappears during the cell cycle in a cyclic manner and that enables or inhibits the enzymes action, as shown in figure 2.2.[12]

To control the transition between phases, cells also developed a set of checkpoints along their cycle. These control the sequence and timing of the cycle, in addition to ensuring that essential events are completed successfully. As such, these checkpoints function as hold points and, in the event that a vital task is not performed correctly, they will delay the cycle's progression until the task is completed.[13]

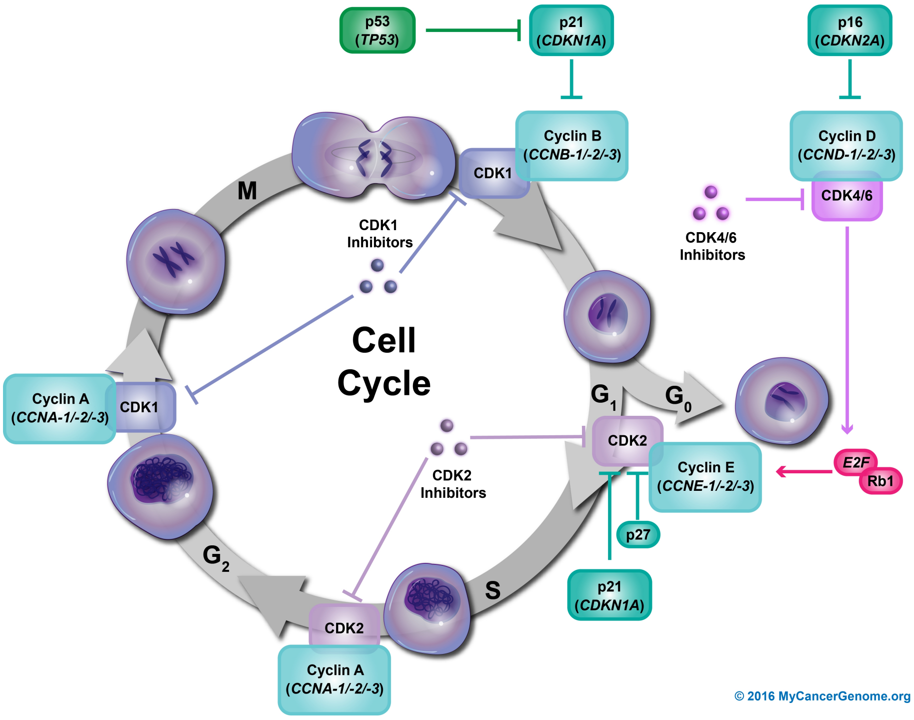

Figure 2.2: Cyclin presence in the ekaryotic cell cycle. Source: [14]

G1 phase

Along with **G0**, this stage of the cell cycle is the only one in which the cells respond to extracellular *stimuli*. As such, this phase is commonly a target for mitogenic signals (cell cycle inducing signals).

At this phase, cells receives intra and external signals to enter a new round of the cellular cycle or to transition into a resting, quiescent state (the G0 phase). If the cell enters a new round is made, the cell becomes unresponsive to external signals until the end of the cellular life cycle.[15]

In G0 and early G1 stage, high levels of CDK inhibitors (CKI) and low levels of cyclins suppress the activity of essentially all CDKs. Due to this inactivity, the retinoblastoma protein (pRb) remains connected to E2F (a protein family), which impedes DNA replication and places the cell in resting state. However, upon correct extra cellular stimuli, D-type cyclin starts to accumulate. This cyclin will bind to CDK4/6 enzymes and form a complex that will phosphorylate pRb. In turn, this process releases E2F that will transcribe genes responsible for encoding certain proteins, essential for the transition to the S phase.[15]

CDK4/6 and CDK2, now active due to coupling with cyclin E, deactivate pRb completely and cause a greater expression of E2F-responsive genes, which are required to ”guide” the cell through the G1/S transition. The increase in transcriptional activity induces the creation of more cyclin E, in a feedforward cycle.

At this point, the G1/S checkpoint might be activated due to the absence of mitogenic signals, the presence of anti-proliferative genes or the presence of defective DNA. If such happens, CKIs are used to interrupt the cell cycle. [15]

S phase

After G1, cells enter the synthesis phase, or the **S phase**, so called due to the DNA replication which occurs during this stage, a process that starts after DNA replication proteins achieve a satisfactory level.

To ensure that DNA replication occurs in a reasonable time-frame, the process is initiated in multiple ”origin points” of the chromosomes simultaneously. Nonetheless, supervising mechanisms have to be employed to ensure that the cells DNA content is duplicated only once and that it only restarts after the complete cell division. This is achieved by the so-called ”replication licensing system”, which is illustrated in figure 2.3. [15]

This mechanism ensures that the thousands of ”origin points” are utilized efficiently and safely, since even a small mistake during the DNA replication, be it over-replication or under-replication, could result in severe consequences for the cell. As such, precise chromosome duplication must be performed, and it is achieved by the separating DNA replication initiation into two stages.

The first stage takes part early in the cell cycle and ”licenses” the ”origin points” by loading a pre-replicative complex to the DNA. This complex is initially formed by an origin recognition complex to which MCM (mini chromosome maintenance) proteins are added. The second stage takes part in the S phase and promotes the initiation of the replication process at each licensed origin point. Once the replication begins, the MCM complex is removed from each origin point, effectively unlicensing it.

DNA replication can only be performed with an MCM complex, and these complexes can only be loaded into the chromosomes during stages that have low levels of CDK activity. The only moments in the cell cycle that possess such a low level are the final part of mitosis and the beginning of the G1 phases, which ensures that DNA replication can only be started once in each cell cycle. After completing DNA replication the cell enters the Gap 2 phase. [15, 17]

G2 Phase

The G2 phase is the last step ahead of actual cellular division. As such, before progressing any further the cell must ensure that not only the genetic material is correctly duplicated, in the form of sister chromatids, but also that essential cellular structures, such as centrosomes, are too.

Incomplete DNA replication or damaged DNA will trigger checkpoint pathways that will cause cellular arrest in the G2 phase. Such pathways include the ATM (ataxia telangiectasia mutated) and ATR (ATM and Rad-3 related) pathways, which, when activated, provoke phosphorylation of human checkpoint kinases (Chk1 and Chk2).These kinases induce inhibitory phosphorylation of the CDC25 phosphates,

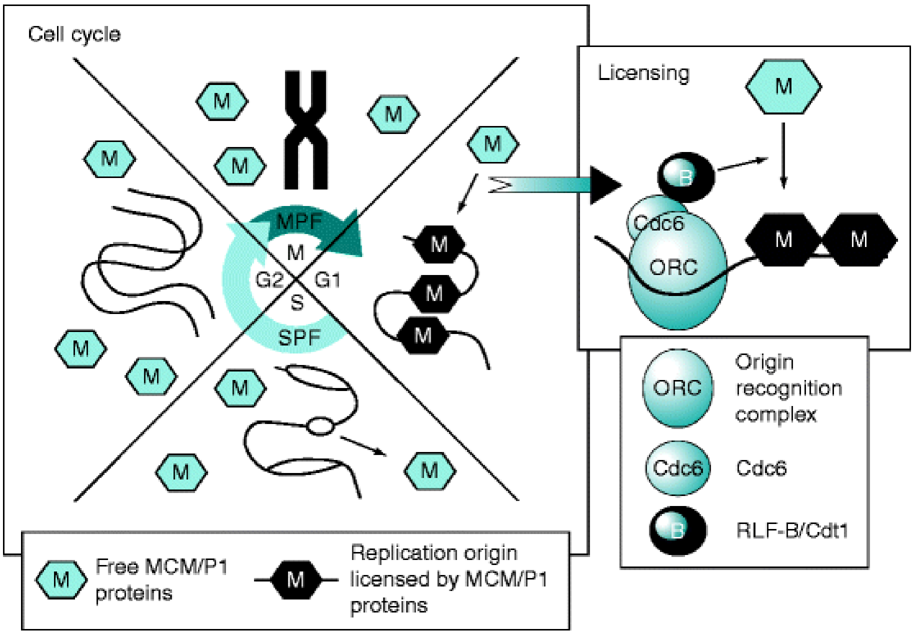

Figure 2.3: Ilustration of the replication licensing mechanism. Source: [16]

in addition to creating a binding site for the 14-3-3σ protein to bind to the phosphates. All this activity will keep the CDK1 inhibited and prevent the transition to the mitosis phase.

Besides the common biochemical processes of phosphorylation/ dephosphorylation, at this point, the cell possesses other arrest mechanisms based on the intracellular location of certain molecules. A good example, is the CDC25 phosphate. Normally residing in the nucleus and driving the cell forward, this phosphate is not only inhibited by the process mentioned previously, but also by the formation of the complex CDC25/14-3-3σ, which is driven by the cell to the cytoplasm where the phosphate can no longer affect the cell progression. Similarly, 14-3-3σ binds with the CDK1/Cyclin B complex and is pushed outside the nucleus, helping to maintain a G2 phase arrest. [15]

M Phase

The **M phase** is the final stage of the cell cycle, after which two daughter cells will have been generated from one parent cell. This is done through two processes, mitosis and cytokinesis, that, combined, constitute the **M phase**. [15].

Mitosis is the process responsible for the separation of the cell's nucleus in two and it is comprised by 5 different stages, as illustrated by figure 2.4, each involving characteristic steps to align and separate the cell's chromosomes:

Prophase Taking place immediately after the G2 portion of interphase, prophase is the initial stage of mitosis. During this stage several DNA binding proteins condense the genetic into X-shaped chromosomes with their identical sister chromatids bound at a common point, the centromere. Simultaneously, the cell's two centrosomes migrate towards opposing poles and several microtubules start emerging from these organelles. These microtubules are collectively called spindle and will form a network that will pull apart the duplicated chromosomes.

Prometaphase After the conclusion of prophase, prometaphase ensues. During the course of this phase, the cell's nuclear membrane collapses into various small vesicles that grant the mitotic spindle access to the chromosomes. The microtubules are highly dynamic and seek to locate a chromosome by growing outwards from the centrosome and then collapsing backwards. When at least one microtubule from each centrosome has connected to the kinetochore (protein complex at the centromere) of every chromosome, a tug of war begins as the chromosomes move back and forth between the poles.

Metaphase As metaphase begins, the chromosomes position themselves along the cell's equator. Each of them connected to at least two microtubules, one to each pole. As the tension applied on the spindle balances itself, the chromosomes cease to move back and forth between the centrosomes. Furthermore, at this point the spindle has developed three groups of microtubules. The **kinetochore microtubules** connect the chromosomes to the poles, the **interpolar microtubules** reach for the opposing pole, passing through the equator and the **astral microtubules** extend from the poles to the cellular membrane.

Anaphase Metaphase gives way to anaphase as the chromosomes separate and start moving towards the poles. The enzymatic breakdown of cohesin (the protein responsible for linking both sister chromatids together during prophase) is the event responsible for this separation, which makes each chromatid an independent chromosome. The chromosome migration is made possible by the variation in micro tubular length, that divides anaphase into 2 stages.

During the first stage, or anaphase A, the kinetochore tubules shorten and pull the chromatids, now turn chromosomes, towards the poles. After this initial stage, during anaphase B, the astral microtubules pull the poles further apart causing the interpolar tubules to slide past each other and exert extra pression on the chromosomes.

Telophase During this stage the chromosomes reach the poles and the mitotic spindle disassembles. As this happens, the small vesicles containing the destroyed nuclear membrane surround both sets of chromosomes. After the dephosporylation of these vesicles, a new nuclear membrane is formed around each group of genetic material.

When the last stage of mitosis has ran its course, the cell possesses two nuclei with identical genetic material and it is time to split the parent cell into two identical daughter cells, a process called **cytokinesis**.

This physical mechanism begins with the cell pinching itself at the equator forming a cleft called **cleavage furrow**. This cleft is formed by the action of a contractile ring consisting of overlapping actin and myosin filaments. As the ring tightens, it eventually reaches its smallest point. At this moment, the cell bisects itself forming two daughter cells of equal size. [18]

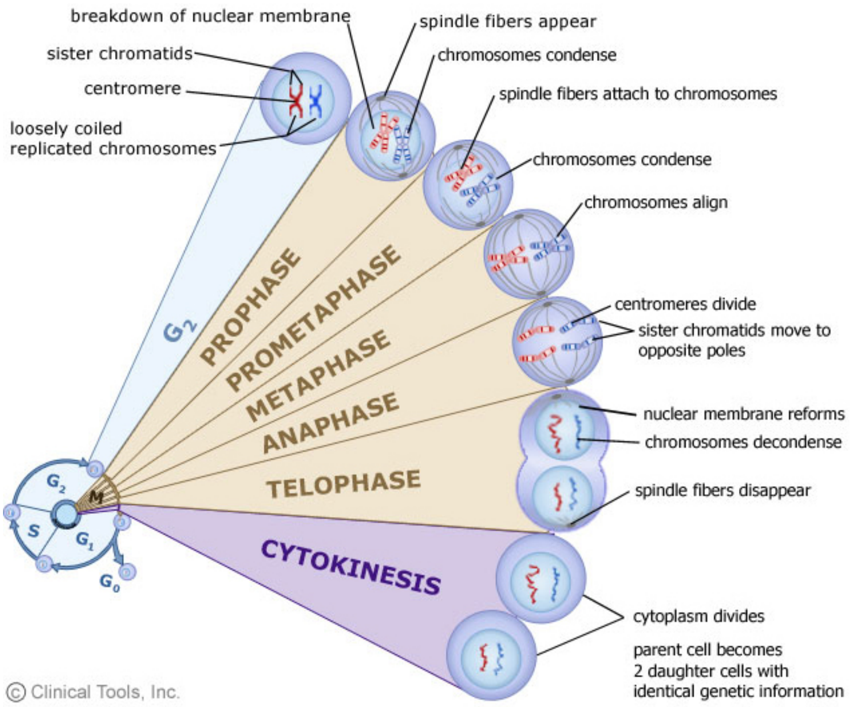

Figure 2.4: Mithotic phases of the cell cycle. Source: [19]

2.1.3 Cell Imaging

As section 2.1.2 made clear, the cell cycle is a complicated process, driven and regulated by an intricate system of protein complexes that trigger specific events at specific times.[20] Being able to observe the changes in cellular structure caused by these mechanisms plays a key role in understanding how they operate. As such, the technology to observe cells needs to constantly improve producing techniques such as **fluorescence microscopy**.

Fluorescence microscopy

Most improvements in microscope technology focus on improving the contrast between the relevant observations and its background. Fluorescence microscopy contributes to these advances by providing a technique that attempts to only reveal the objects of interest on an otherwise black background.

To do so, it is required that the objects of interest fluoresce. Strictly speaking, fluorescence describes photoluminescence that occurs when materials absorb photons at a certain wavelength and then emit photons on a different band of wave-length.

The fluorescence phenomenon can be illustrated through a Jablonski diagram, present in figure 2.5, which describes the photo physical processes in molecules. In figure 2.5, $S_1,\ S_2,\ S_3$ represent various energy levels at which can reside outer electrons. S_0 corresponds to the ground state, representing the level of energy a molecule possesses if it is not being excited by light. On the other hand, S_1 and S_2 represent excited states, where S_2 corresponds to a higher energy level than S_1.

When the molecules absorb light, all the photons' energy is absorbed. If the energy contained in

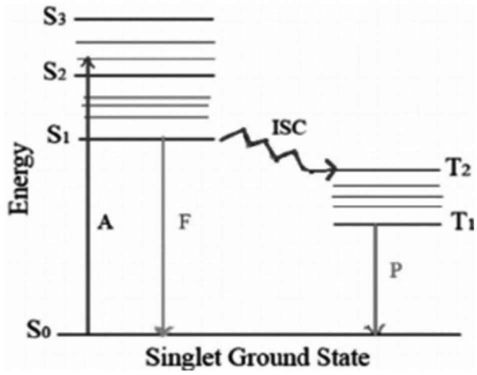

Figure 2.5: Jablonski diagram. A-Absorption, F-Fluorescence, ISC-Intersystem Crossing, P-Phosphorescence, S_0-Ground state, $S_{i]}$-Higher energy states, T_i-Triplet state. Source: [21]

a single photon is equal or greater than the energy gap between the different levels, the molecules electrons will transition to a higher energy state (from S_0 to S_1 or S_2, for example). A photon's energy can be determined by Plank's formula:

$$E = \frac{h \times c}{\lambda} \tag{2.1}$$

where E is the photon's energy, h is Plank's constant, c is the speed of light in vacuum and λ is the photon's wavelength. As equation 2.1 clearly states, a photon's energy is dependent only on its wavelength, which means only a certain interval of the electromagnetic wave spectrum can ”boost” a molecule's electrons to a higher energy state.

Once it transitions, the excited electron is released to the lower energy level on the excited orbit, through mechanisms such as internal conversion or vibrational relaxation. From this lower level of the excited state, the electron returns to the ground state. In doing so, energy is released in a form of a photon in a different wavelength from the one absorbed (due to the energy lost at the excited state) and fluorescence occurs. The difference between the wavelength of the absorbed photon and the one emitted is called Stokes-shift.

Nonetheless, the fluorescence phenomenon is only useful if the target molecules ”light up”. Whereas many organic substances possess natural fluorescence, the common approach from fluorescence microscopy is to use synthetic compounds that bind to a specific biological molecule and have great fluorescence properties. These compounds are known as fluorophores and provide a targeted approach since they grant the ability to only mark relevant biological molecules. [22]

DAPI Stain

One of the more relevant aforementioned fluorophores is the 4',6-diamidino-2-phenylindol or DAPI stain. This staining compound is widely used to mark DNA since it binds weakly to RNA and strongly to AT rich DNA regions. This strong cohesion grants it a high sensibility that allows for the observation of even small DNA quantities such as the one contained in virus and chloroplasts, hence its common utilization.

The staining process associated with this fluorophore is simple and requires no hydrolysis, with the stain being manually applied by pores made in the cellular membrane. When excited by light it emits a strong white blueish fluorescence, pictured in figure 2.6, with its emission maximum placed at 461 nm and its absorption maximum placed at 358 nm. [23, 24]

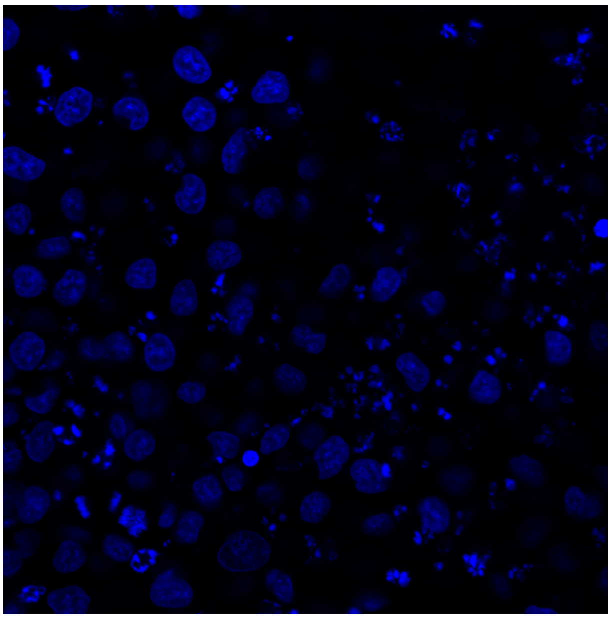

Figure 2.6: DAPI stained cell culture.

2.1.4 Current cell staging techniques

Cell staging techniques have changed and advanced along the years. Amongst the more recent ones, two of them present very different approaches with both yielding significant advantages:

- The first, presented in [25], relies on the use of biological markers and fluorescence microscopy to identify the stage of any given cell.

  Identifying antiphase oscillating proteines that mark cell-cycle transition and encoding them with fluorescence probes made visualizing a cell's current stage possible. Each color represented a different stage, cells in the G1 phase presented a red nucleus while the cells in S, G2 or M phase presented a green nucleus, as shown in figure 2.7. From the figure, it is also clear that the transition from G1 phase to the S phase is marked by a temporary yellow colored nucleus, at which point the cell has already entered the S phase.

  This technology, called **FUCCI** (fluorescence ubiquination cell cycle indicator), uses dual-color imaging with bright contrasting colors that do not clash with most modern markers Furthermore, the very different colors of its markers allow for *in-vivo* observation of temporal and spatial patterns. Nonetheless, this technique is expensive and must be applied to a live cell culture before any imaging is performed which means it cannot be used to classify former cell cultures and since the yellow marker for the S phase shown in figure 2.7 is only temporary, only binary classification is possible (G1 and S/G2 phase)

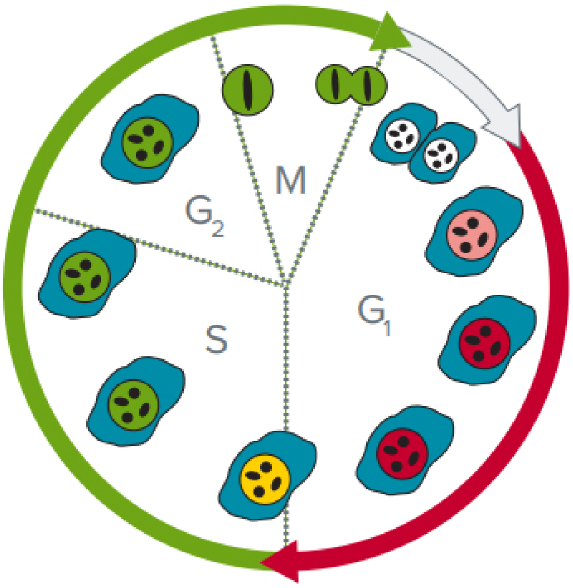

Figure 2.7: FUCCI staining process:Cells appear green if they are in phase G1 and red if they are in phase S/M/G2. Source:[26]

- The second technique, presented in [5], stages a cell by estimating the DNA content of cells through fluorescence microscopy and image analysis.
  This method starts with images of DAPI stained cell cultures and performs a nuclear segmentation for each cell. After this initial step, the method has the nucleus of each cell isolated and estimates the DNA content through its brightness. Then, the population of each phase (G1, S or G2/M) is estimated by applying thresholds to the DNA intensity or by modeling the DNA intensity histograms produced with cell cycle analysis tools.
  This method possesses the advantage of relying on a simple and widely used marker, the DAPI stain, and does not require any special procedure to be performed on the cell culture, apart from image acquisition, and can be performed on previous cell cultures. However, it relies on a population based analysis and is incapable of staging or tracking a single cell, one of the advantages of the first method.

2.2 Machine Learning

The search for patterns in data is a fundamental problem that has a long and successful history, one that culminated in Machine Learning (ML). Machine Learning consists of classification and prediction algorithm that adjust their parameters according to the properties of a training set, giving computers the ability to learn without specific programing. [27]

As stated in 1.1, this thesis intends to classify cells. As such, only the classification scope of Machine Learning will be of interest. To solve the classification problems, the goal is to tune the used model so that each input is assigned to one of a finite number of discrete categories.

The stage during which a model tunes its parameters is called learning phase, and it is followed by the testing phase. During the latter stage, the algorithm attempts to classify a new set of data. A model's capability of correctly classifying never before seen data is called generalization, and it is one of the essential goals of any ML problem.

These classification problems can be divided into two, supervised and unsupervised problems, depending on the shape of the training set [28]. In unsupervised learning problems, the training data consists only of input examples. It is lacking a corresponding target value that, in classification problems, corresponds to the intended class of the input. In unsupervised learning problems, a typical problem consist of finding similar examples amongst the data, a process called clustering. On the other hand, supervised learning problems possess a training set with examples of inputs and their corresponding target output. [27]

For this thesis, the training set had a classification for each input example, as such, supervised learning was adopted.

2.2.1 Deep Learning

Most classification problems can be solved with the correct set of features extracted from the data and analyzed by a machine learning algorithm, the difficulty lies in choosing the relevant features and how to extract them, in other words how to represent the data in meaningful way.

The solution is to use machine learning not only to map the relation between representation and output, but the representation itself, a process called representation learning. However, in real-world applications, it can be very difficult to extract high-level, abstract features from raw data which turns the representation into a problem as hard as the original one.

Deep Learning is a subset of machine learning and presents a solution by introducing representations that result from automated processes. That is, deep learning provides a system built with a cascade of trainable modules. By training this system end to end, each module will adjust itself to produce the correct answer. This method allows the system to learn how to represent the raw data and how to solve the problem provided. [29]

This novel approach has produced significant advances in the artificial intelligence field. With the ability to discover intricate patterns in high-dimensional data, deep learning has been applied in various fields, with outstanding results in image and speech recognition. In particular, artificial neural networks and convolutional neural networks models have produced impressive results in image classification, beating records in established competitions. [30]

Artificial Neural Networks

Artificial Neural Networks (ANNs) are the quintessential deep learning model, yet their goal is not to model the human brain, contrary to what their name suggests. Rather, they draw insights from our knowledge of the brain to achieve models capable of statistical generalization. However, ANNs receive their name from being a network of connected neurons, not unlike the brain.[31]

Each neuron, schematically represented in figure 2.8, receives inputs signals ,x_i, from various other

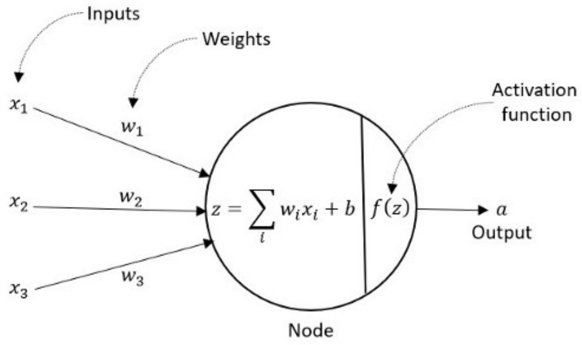

Figure 2.8: Artificial neural network neuron.Source:[32]

units and computes its own output. Each input is regulated by the connection weights, w_i, which emulate biological synapses. Thanks to a activation function, $f(z)$, the neurons possess a non-linear behavior, which is limited by a threshould β. As such, the output of a neuron can be computed as follows: [28, 33]

$$O = f(net) = f(\sum_{i=1}^{k} w_i x_i + b) \tag{2.2}$$

In 2.2 the variable net represents the scalar product of the weight vector and input vectors added to the offset b, while k represents the number of inputs for a specific neuron:

$$net = w^T x = w_1 x_1 + w_2 x_2 + ... + w_k x_k + b \tag{2.3}$$

From equation 2.2 it is also obvious that the activation function will determine the neural output. The simplest case is to consider $f(z)$ as a boolean step function, in which case the output can be described as:

$$O = tf(net) = \begin{cases} \frac{1}{1+e^{-z}}, & if w^T x + b > \beta \\ 0, & else \end{cases} \tag{2.4}$$

In addition to the activation function, the connecting weights also determine the output value. It is by adjusting the weight vector that each neuron is capable of learning. Since the neurons are connected among themselves in a network, as shown in figure 2.9, this learning ability is inherited by the network. [28]

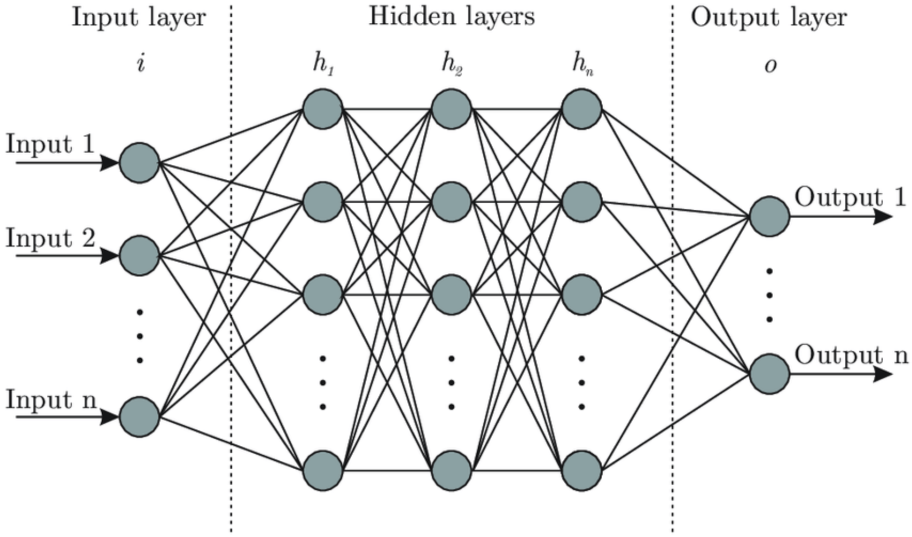

Figure 2.9: Artificial neural network. Source:[34]

As figure 2.9 exemplifies, artificial neural networks are organized in distinct layers. The input layer receives the network's input vector while the output layer produces the intended output. Between these two layers, a model can have multiple hidden layers, depending on its depth. [35] Each neuron connects only to the neurons in the previous and next layer, each connection having a respective connecting weight. To adjust these weights, effectively training the network, a common method is to use back propagation, a method that can be summarized as follows: [36]

- Select the appropriate training set for supervised learning;
- Create the model and randomly initialize the connection weights;
- Select the appropriate error/ loss function, which describes the difference between the desired output and the output produced by the network, E, learning rate, η, and momentum, α (which regulates the impact previous weight changes have on the current calculation);
- Apply weight update, Δw_{ij}, to each target output in all hidden layers and compute associated error value;
- Repeat the last step varying the network's input until the loss function (L) is properly minimized.

The weight update rule can be defined as:

$$\Delta w_{ij} = -\eta \frac{\partial L}{\partial w_{ij}} \sum \alpha \Delta w_{ij}(m-1) \tag{2.5}$$

Where η corresponds to the learning rate which determines the rate of change in the networks weight and α corresponds to the momentum which determines the effect the past $m-1$ weight changes on the current direction of movement in the weight space. E corresponds to the error function, here the binary cross-entropy was used:

$$L = -\frac{1}{O}\sum_{i=1}^{O} y_i \times \log(\hat{y_i}) + (1-y_i) \times (1-\hat{y_i})! \tag{2.6}$$

Where O is the network's output size, y_i is the target value for a certain datapoint and $\hat{y_i}$ is the networks prediction.

As expression 2.5 clearly demonstrates, the appropriate selection of the learning rate and the momentum plays a crucial part in both speed and success of the training.[37]

Convolutional Neural Networks

Convolutional Neural Networks (CNNs) present themselves as an evolution of ”traditional” neural networks. These are a specialized kind of neural networks for processing data that presents a know grid-like topology. Essentially, CNNs are neural networks that possess at least one convolutional layer. That is, at least one layer that uses the mathematical convolution operation instead of a general matrix multiplication. [38]

Standing out as an example of neuroscientific principles being applied to machine learning, convolutional neural networks are capable of extracting local features that depend on sub-regions of data. These local features can later be merged to detect higher-order features and produce relevant information about the data. The use of local features makes these models somewhat invariant to some input changes, since local features that are useful in one region of the data may be used in another region. This is the reason why CNNs were proposed, to create a model that presented some invariance to small input changes. [38, 39]

As stated, CNNs make use of the convolution operation. Mathematically, the convolution expresses the amount of overlap a function g produces as it is shifted over another function f, the product function being a ”blend” of the two.[40]

Commonly, convolution is noted using an asterisk operator. As such it can be expressed as follows:

$$[f * g](\tau) = \int f(\tau)g(t - \tau)d\tau \tag{2.7}$$

When applying convolution to machine learning, the first argument (f in equation 2.7) is called input, the second (g in equation 2.7) is called kernel and the output is commonly called feature space. Also, in machine learning the discreet definition of convolution is used:

$$[f * g](\tau) = \sum_{\tau=-\inf}^{\inf} f(\tau)g(t - \tau) \tag{2.8}$$

In most CNN models, the input is multi-dimensional and the kernel is a multi-dimensional array of parameters tuned by the learning method. Figure 2.10, gives a visual representation of how the convolution operations works in 2-D arrays, as is the case of images.

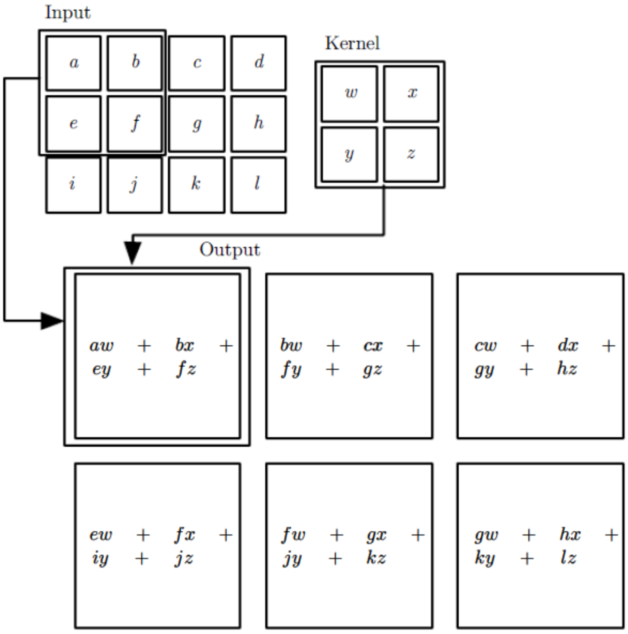

Figure 2.10: An example of a 2-D convolution without kernel flipping. Source:[33]

The use of convolution operations entails 3 concepts that improve machine learning: sparse interactions, parameter sharing and equivariant representation.

In traditional neural networks each output unit interacts with every input unit. However, convolutional networks have sparse connectivity, or sparse interactions. This results from making the kernel smaller than the input, reducing the number of parameters to store and tune and reducing the number of operations required to compute the output and improving the models performance. The graphical representation of sparse connectivity is presented in figure 2.11.

Convolutional networks utilize each member of the kernel at every input position, as shown in 2.10. This is know as parameter sharing and it contrasts with typical neural networks where each connection weight is used once and only once.

Parameter sharing causes the convolutional layer to be equivariant to translation, that is, if the input changes the output changes in the same way. For example, when processing images, convolution produces a 2-D map of where features appear. Equivariance means that if we shift the image, the feature map will be shifted in the same way, keeping the same features as previously. This is useful in situations where the presence of a feature is of relevance and not necessarily its location in the image. [38]

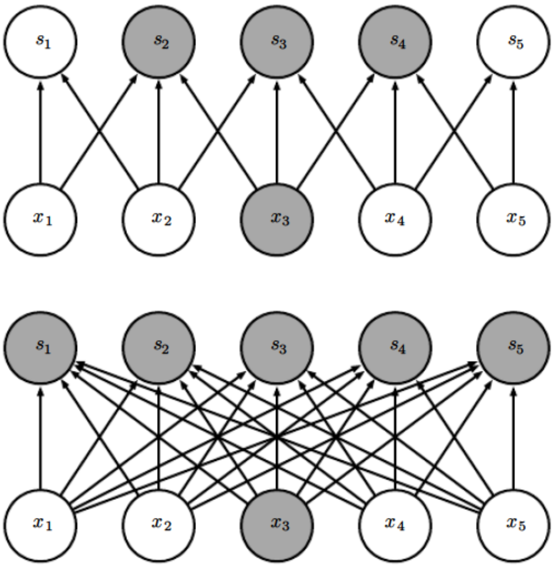

Figure 2.11: Sparse connectivity exemplified: Considering input x_3, when s is formed by a convolution kernel of width 3, only 3 outputs are affected (Top). However, if formed by matrix multiplication, all outputs are affected and connectivity is no longer sparse. Source:[33]

In addition to the convolutional operation, the convolutional layer of a network has two more stages. A detector stage, where each linear activation is transformed by a non-linear function and the pooling stage, where a pooling function further alters the output. Pooling functions replace the output with the a summary statistic of neighboring outputs, merging semantically similar features into one. A CNN may have one or multiple convolutional layers, whose structure is represented in 2.12, depending on the complexity of the model. This convolutional stage of the model is connected to an artificial neural network and the entire model is trained using the back propagation method, similar to the explanation provided in the previous section. [30, 38]

Convolutional neural networks have enjoyed relative success in detecting, segmenting and recognizing objects since the early 2000's. Nonetheless, they were largely forgotten by the computer vision community until the ImageNet competition. In this competition (which consists in using machine learning algorithms to classify a large image dataset in one thousand classes) CNNs performed remarkably, achieving extraordinary results and thus becoming the standard approach for computer vision problems. [41]

As such, to reach the proposed goal of classifying the cellular phase of single cells relying on intracellular features, DAPI stained images from a FUCCI culture were obtained and used to train deep learning algorithms, particularly an ANN and a CNN.

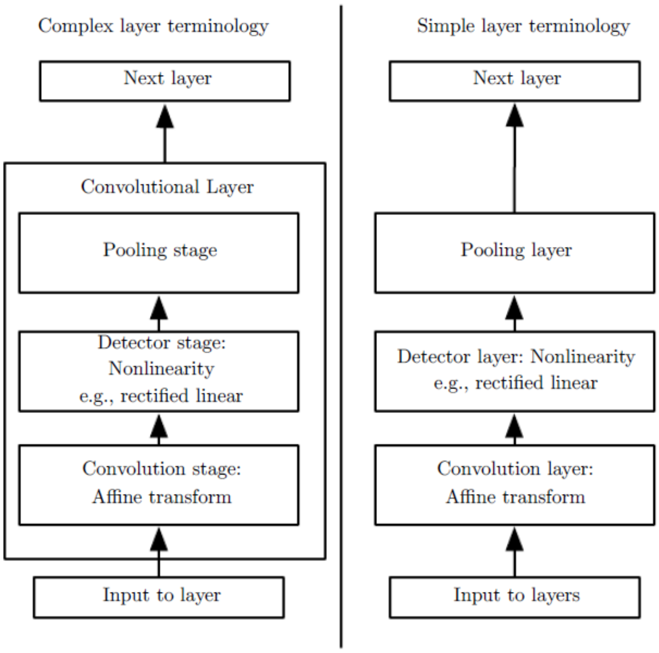

Figure 2.12: Components of a typical convolutional neural network layer. Source:[33]

Chapter 3

Methodology

3.1 Biological Material and Data

In this section a brief explanation on the processed biological data that was the basis of the work performed in this thesis will be given. Most of the work was performed prior to this master thesis and provided the initial data used during this project.

Additionally, an explanation of the deep learning methods used during this project will be provided. All of the artificial intelligence methods were implemented in Python utilizing the Keras and Tensorflow libraries.

3.1.1 Cell culture and imaging

Even though only the DAPI staining information was used to identify the features that reflect the cells progress along the cell cycle, fluorescence imaging provided the basis for this work. In total, 836 images were obtained from 12 samples comprising 5873 cells from NMuMG-Fucci2 *in-vitro* cultures were obtained from Riken institute Japan.

Following the process described in [42], cells were grown in Dulbecco's modified eagle medium (DMEM) supplemented with 10% fetal bovine serum, 10% penicillin/streptomycin, and 10 σ g/ml insulin. After being washed with a solution of phosphate buffered saline (PBS), the culture was fixed with a solution of 4% formaldehyde in PBS for 15 minutes at room temperature in the dark. Cells were then quenched, subsequently permeabilized and their fixed nuclei stained with DAPI at room temperature in the dark. The coverslips were then mounted on slides using Vectashield plain mounting medium. The prepared slides were kept at 4 $^{\circ}$ C and protected from light prior to imaging [43].

To extract all the information contained of the DAPI stained nuclei, multiple images were taken along the z axis and merged together by projecting into a single image.

3.1.2 Image Pipeline

The images obtained from the fluorescence imaging were then processed to produce the data used as starting point for this thesis. The preprocessing work was performed before this thesis and a brief explanation will be provided based on [43].

The image preprocessing pipeline described in figure 3.1 was used to process each FM image produced. The pipeline consists of two steps, an initial application of a denoising algorithm and contrast/ intensity adjustments followed by the segmentation of each nucleus.

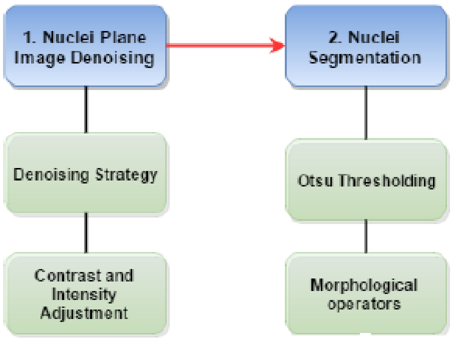

Figure 3.1: FM images preprocesssing pipeline. Source:[43]

Nuclei plane image denoising

Denoising is used in image processing to reduce the effect of noise generated by the instrumentation systems into the samples and to emphasize the underlying relevant data [44].

The noise introduced in fluorescence microscopy follows the poison distribution, with a probability function that can be defined as:

$$Pr(X = k) = \frac{\lambda^k exp^{-k}}{k!} \tag{3.1}$$

where λ is the distribution parameter.

A Bayesian algorithm was employed to remove the noise with maximum-a-posterior optimization criterion:

$$\hat{Z} = argmin_z E(Z, Y) = argmin_z(E_y(Z, Y) + E_z(Z)) \tag{3.2}$$

where $E_y(Z, Y)$ is the data fidelity term and $E_z(Z)$ the prior term regularizing the solution required to introduce some *apriori* information about the solution. Assuming observations are independent and the noise compliant with a Poisson distribution, the data can be described as:[45]

$$E_y(Z, Y) = -\log\left[\Pi_{i,j=0}^{N-1,M-1} p(Y_{i,j}|z_{i,j})\right] = \sum_{i,j=0}^{N-1,M-1} |z_{i,j} y_{i,j} \log(z_{i,j} + C|) \tag{3.3}$$

where C is constant.

The distribution in 3.3 is denominated by a $\log$ total variation potential function:

$$TV\log = \sqrt{\log^2 \frac{z}{\varsigma}} \tag{3.4}$$

where z and ς are neighboring pixels.

The function described in 3.4 has efficient high frequency noise removal in homogenous regions and a smaller penalization in sharp transitions, useful for biological images who possess abrupt transitions that are desired.

Segmentation

With the segmentation process, the cell culture images were divided into multiple images, each containing a nucleus of a cell. This process has a typically low accuracy and inconsistent output when applied to most images, and is crucial to ensure the success of the final analysis.

For this data, the segmentation strategy was used in the denoised and contrast/ intensity DAPI plane (blue channel) of the FM images, and consisted in the application of Otsu thresholding and morphological operators to each image [43].

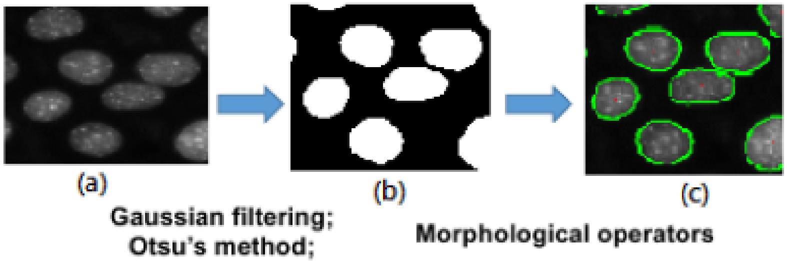

Figure 3.2: Overview of the cell nuclei segmentation procedure. (a)-Input DAPI image; (b)-Unique mask for each cell; (c)-Obtained boundaries in the original image Source:[43]

After all this processing was applied to each image, the data obtained was stored in a matlab file containing a pixel map for each nucleus and the corresponding binary classification from the FUCI method described in 2.1.4. The information stored in these Matlab files formed the initial dataset for this thesis, comprising of 5873 gray-scales images (since only the blue channel information was utilized) of the various nucleus contained in the initial images.

This dataset was further divided into a training dataset (90% of the dataset) and a validation dataset (10% of the dataset).

3.2 Methods

3.2.1 Machine Learning

To determine the cellular stage of each cell and have the ability to classify each nucleus independently (i.e. not rely in clustering methods), machine learning algorithms were employed. Namely artificial neural networks (ANN) and convolutional neural networks (CNN).

Neural Networks

Feature extraction The first step in using an ANN to learn the cellular stage, was to select and extract relevant features from the dataset. As described in 2.1.2, one of the key defining characteristics of the progression along the cell cycle is the variation of genetic material. In particular, the duplication of DNA is a key characteristic of the S phase as is the growth of the nucleus in the G1 and G2 phases.

As such, the variation of genetic material contained in the cell and the variation of the nucleus size were selected as the defining characteristics to express the cellular stage. To translate this behavior into features capable of being used in training an ANN, the area and intensity of the nucleus were selected.

Each feature was expressed mathematically. The area was defined as the total number of pixels contained in a nucleus (NP) limited by boundaries i' and j' such as:

$$Area = \sum_{i<i',j<j'} NP_{i,j} \tag{3.5}$$

The total intensity was defined as the sum of the intensity of each pixel in the nucleus (as shown below) and, theoretically, reflects the amount of DNA contained in each cell.

$$Area = \int_A intensity dA = \sum_{i=1}^{T} Intensity_i \tag{3.6}$$

By plotting each nucleus' intensity and area, as shown in figure 3.3, one should expect to identify three different concentrations of points:

- a first group of cells in G1 phase, with a significant rise in area and intensity, characteristic of cell growth
- a second group of cells in S phase, with constant area and intensity increase which represents the DNA duplication that occurs during this phase
- a third and final group of cells in G2 phase, with almost double area and intensity than in G1 which represents the cell's final growth corresponding to this phase

Data normalization After extracting the features, data normalization was applied to the data set, namely, z-score normalization.

Data normalization is a common pre-processing technique to minimize the impact features with different ranges have in the final outcome. Potentially, features with larger ranges would have a higher

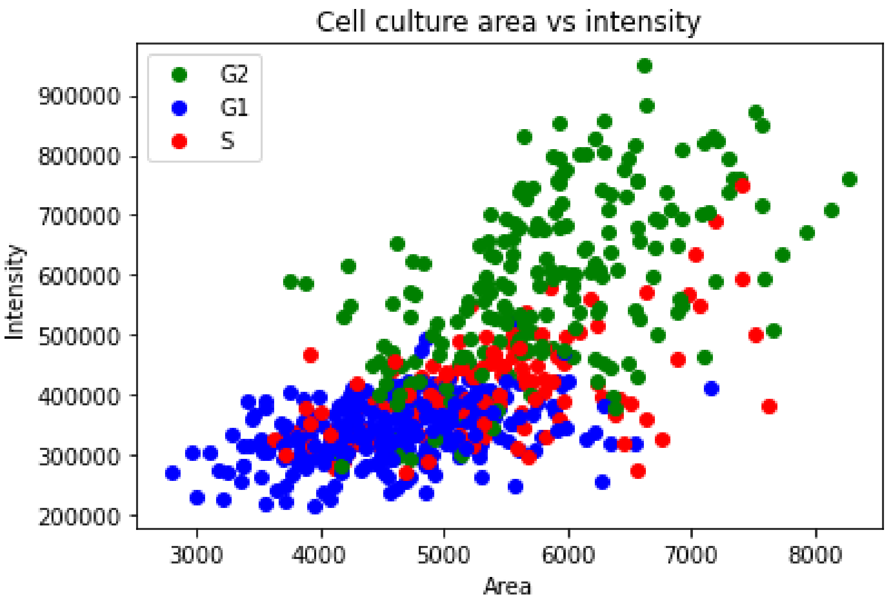

Figure 3.3: Scatter plot representing area and intensity of biological data

contribution for the final outcome than the features expressed in a smaller range. Furthermore attributes should be dimensionless so that the unit of measure does not impact the final output. As previously stated the method used was the z-score normalization, which can be defined as [46]:

$$x_{ij}^* = \frac{x_{ij} - \tau_{ij}}{\sigma_j} \tag{3.7}$$

where x_{ij}^* is the normalized attribute value, x_{ij} represents the raw data and τ_j and σ represent the mean and standard deviation (STD) for the values of the j^th attribute. Z-score normalization returns a dataset with 0 average and standard deviation of 1 and is one of the most commonly employed standardization techniques. [47, 48]

Designing and training the ANN With the features extracted and the visual classification from the FUCCI method, a supervised learning method was employed to train an ANN.

To size the required network it was first created a network that could ”memorize” the problem, i.e. overfit the dataset, and then overfitting prevention methods were applied. For this, the drop-out technique was employed.

In this method the term dropout refers to ”dropping” units in a neural network along with incoming and outgoing connections, as shown in figure 3.4. The choice of which nodes to drop is random, with a fixed independent probability of p for each unit to drop. p can be selected from a test dataset, however a probability of 50%, i.e. $p = 0.5$ seems to be optimal for most neural network problems [49].

By dropping units, essentially a thinned network is trained each time and is formed by all the remaining units. As such, training a network with elements can be seen as training a set of 2^n thinned networks with weight sharing.

This approach poses the problem that at test time it is not feasible to express the average output of so many thinned layers. However, a good approximation is to use a neural network without the dropout where the weights of each hidden unit is multiplied by p at validation time [49]. This simple averaging method ensures that the expected output of each hidden unit at test time is the same as during the training phase. Thus, effectively combining 2^n networks into a larger single neural network that can be used at test time.

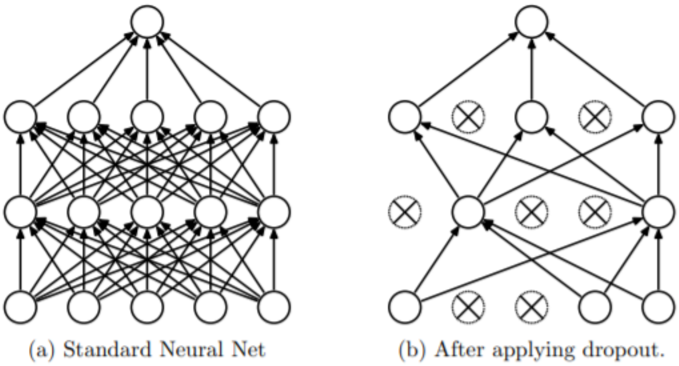

Figure 3.4: Dropout Neural Net Model. Left: A standard neural network with 2 hidden layers. Right: An example of a thinned net produced by applying dropout to the net network on the left. Source:[49]

To adjust the training of the designed network 3 parameters were adjusted [27]:

- **Epochs** - Parameter that defines the number of times the learning algorithm will work the entire data set
- **Batch size** - Parameter that defines the number of samples that are processed before the model is updated
- **Learning rate** Parameter that defines how much the weights in a neural network are updated on each batch
- **Learning rate** Parameter that defines how much the weights in a neural network are updated on each batch
- **Loss function** Parameter that defines how the error or loss is determined with each batch

These parameters are correlated among them, for example, smaller learning rates require more training epochs since each update has a smaller effect on the weights. On the other hand, batch size determines the number of times the error function is determined per epoch and subsequently the number of times the model weights are updated in each epoch.

There is no exact way to determine the value for each one of the parameters, with an empirical process being required to determine the best solution for each problem. In the context of this thesis, after various tests a large number of epochs were used in conjunction with overfitting prevention methods and the mini-batch gradient descent method was used [50] (when batch size is smaller than the sample size, resulting in multiple batches per epoch) with a small learning rate to ensure convergence.

For the loss function, binary cross entropy loss function was used and it can be defined as:

$$CE = \begin{cases} -log(f(s_1)) & if \quad t_1 = 1 \\ -log(1 - f(s_1)) & if \quad t_1 = 0 \end{cases} \tag{3.8}$$

where s_1 and t_1 are the score and the ground truth label for the class C_1, and where $t_1 = 1$ means that class $C_1 = C_i$ is positive for this example. [51]

In addition to minimizing the loss function, the overall accuracy of the model was also monitored during training, which can be defined as:

$$Accuracy = \frac{TP + TN}{TP + TN + FP + FN} \tag{3.9}$$

where TP is true positives, FP is false positives, TN is true negatives and FN is false negatives.

In the end, an ANN with 10 layers of 1000 elements each was trained and optimized using the *Adam optimizer*.

Convolutional Neural Networks

Image generation Contrary to ANN's, and as explained in chapter 2, CNNs are capable of feature detection and selection. As such, instead of extracting the features, as done for the ANN method, 150×150 pixel images were produced from the information contained in the Matlab files generated by the preprocessing pipeline previously explained in this chapter and used as input. Figure 3.5 represents one of the images generated for every nucleus contained in the information.

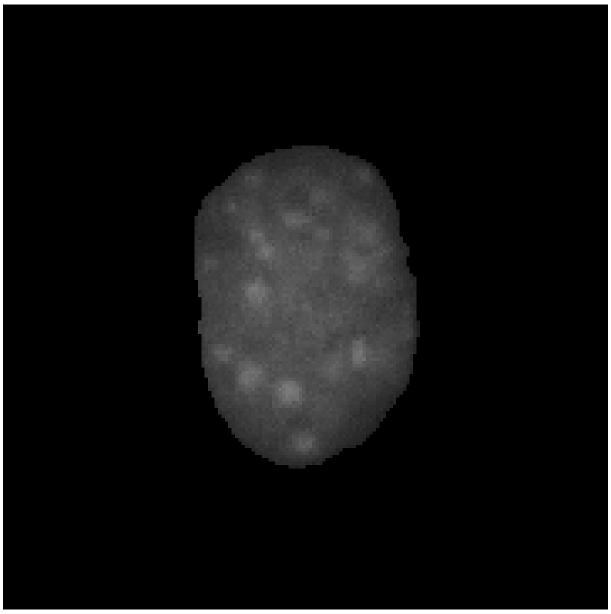

Figure 3.5: Image generated from processed pipeline and used as input for the CNN.

Data augmentation The use of CNNs for image classification requires a large amount of data to prevent overfitting. Unfortunately, the original data set only presented 5873 nucleus and, as such, data augmentation, a data-space solution to the problem of limited information for deep learning, was employed during this work.[52].

While not the only solution to overfitting in deep neural networks, data augmentation addresses the problem at its root, the training data set, by assuming more information can be extracted from the original data through augmentation. To extract this additional information, data augmentation methods typically inflate the training dataset size by either data warping or oversampling, with techniques from geometric and color transformations to random erasing, adversarial training or neural style transfer. [52]

During this project, and since the two classes considered were balanced in the available data-set , only data warping was employed. However, the main goal of data augmentation is to inflate the available data while keeping the label of each data point valid. Below are some descriptions of geometrical transformation techniques [52]:

- **Flipping** - Flipping corresponds to the transformation where an image is flipped across either on the horizontal axis, the vertical axis or both;
- **Color space** - Color space augmentation describes techniques where color channels are manipulated. One simple example of these techniques is isolating only of the RGB channels or changing the intensity values of a image describing color histogram;
- **Cropping** - Cropping corresponds to extracting a patch from the total image. It is particularly useful in processing images with mixed height and width dimensions;
- **Rotation** - Rotation corresponds to rotating the image either left or right on an axis between 1° and 359° ;
- **Translation** - Translations are performed by moving the image up, down, right or left, and are particularly useful in removing positional bias from the images;
- **Noise injection** - Noise injection consists of injecting a matrix of random values usually drawn from a Gaussian distribution.

Since the two most relevant features for describing the progression in the cell cycle are area and intensity a careful selection of the techniques employed is required to ensure these features are not perturbed and negatively affect the outcome. As such, from the methods described, only rotation, flipping and translations did not affect the area and intensity of the images used.

Designing and training the CNN While data augmentation prevents overfitting and helps the network ”learn” more robust features, it is not the only overfitting prevention method available. In addition to the dropout method previously described, early stopping was used to ensure the designed network would be perform optimally. This method consists of monitoring the validation accuracy and loss to detect overfitting and training is then stopped before convergence [53].

These methods were then used to develop a simple CNN network with only 2 fully connected convolutional layers and 1 hidden layer of 256 nodes, which was trained utilizing a large number of epochs with the mini-batch gradient descent method, binary cross entropy loss function and Adam optimizer, similarly to the training process used with the ANN.

3.3 Validation

3.3.1 MNIST dataset

While the MNIST dataset presents a different problem (multiclass vs binary classification, gray-scale vs binary input) and input structure, this dataset was utilized to understand and validate the design methodologies used. As such, both an ANN and CNN networks similar to the ones used were tested against the modified National Institute of Standards and Technology (MNIST) data set [54]. This dataset contains images from handwritten digits and is one of the most common starting points for neural networks with the performance of various types of networks well documented.

The MNIST was derived from the original NIST and contains a total of 60,000 training images and 10,000 test images, obtained from the same distribution. The data was normalized into black and white digits, and centered in a fixed size image where the center of gravity of the intensity lies at the center of the image[54], which is translated into a 28 × 28 grid where each value is binary. This relatively simple database is ideal to test and validate methods since students and educators of machine learning can benefit from a rather comprehensive set of machine learning literature with performance comparison readily available.

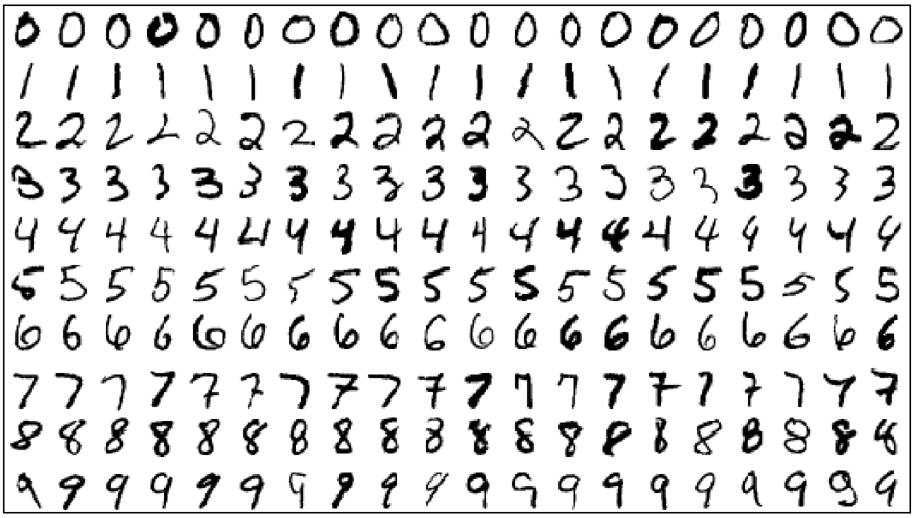

Figure 3.6: MNIST database image sample. Source:[55]

By testing both the ANN and CNN networks with this data set, a validation error of <8% was achieved for both of them. While below the results already achieved by other networks, the goal was simply to validate the training and design methods and no fine-tunning was performed to increase the accuracy on this dataset.

3.3.2 VGG Network

In addition to using the MNIST data set for validation, a pre-trained VGG network was used as a benchmark for the convolutional neural network.

The VGG network has an architecture with very small (3x3) convolution filters followed by sixteen to nineteen weight layers and was proposed for the ImageNet challenge [56]. This challenge uses a sample of the ImageNet dataset of approximately 1000 categories with 1000 images per category. The VGG was submitted for 2014 challenge by K. Simonyan and A. Zisserman from the University of Oxford and achieved 92.7% top-5 test accuracy in that competition. This represented an improvement over prior-art (namely the AlexNet [57] network) and has become one of the benchmark networks for this challenge.

While the ImageNet challenge has a larger dataset and is not exactly comparable to the data available for this project due to the difference in input format and number of channels used, the availability of various configurations of pre-trained VGG16 networks and the widely available bibiography on this network led to its choice as a benchmark.

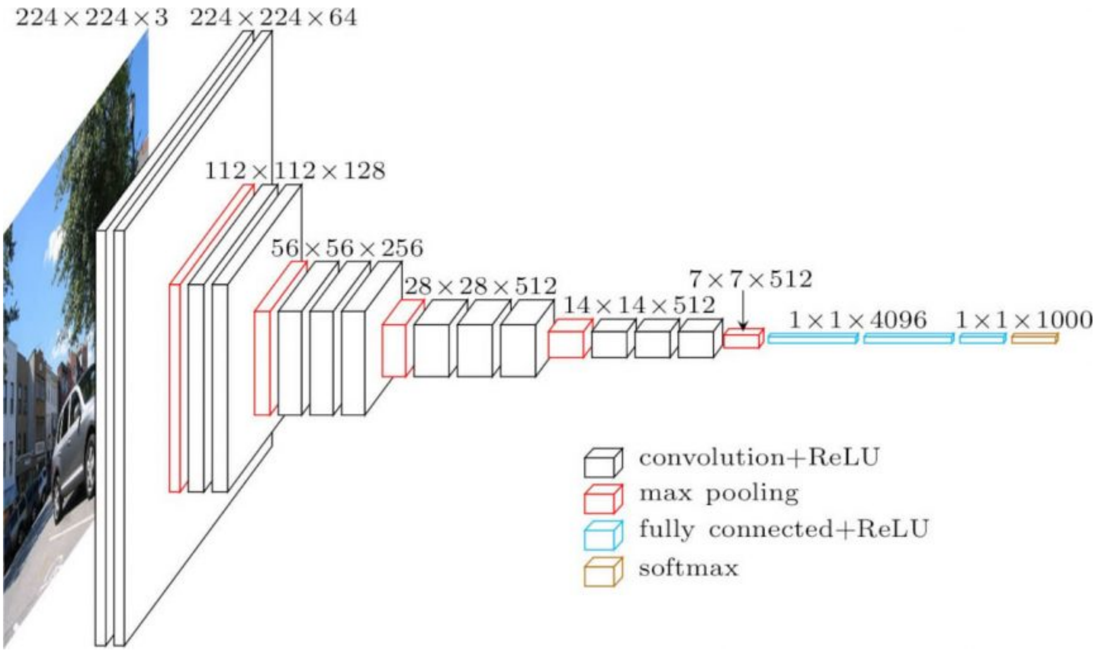

Figure 3.7: VGG16 architecture. Source:[58]

Chapter 4

Results

In this section, the results obtained during this work are presented. First, the results for the artificial neural network are shown with a demonstration of the overfitting prevention methods followed by the demonstration of the results obtained utilizing the convolutional neural network.

4.1 Artificial Neural Network

On this section, the results obtained during the use of artificial neural networks will be demonstrated, both the efficiency of the overfitting prevention methods and the overall result from the trained network.

After extracting the selected features from the biological dataset, area and intensity, these were subjected to classification using an artificial network. As illustrated in figure 4.1, the designed network was capable of overfitting the problem. This is evidenced by the separation between the validation loss and the training loss represented in figure 4.1(a).

Figure 4.1(b) represents the accuracy evolution of the same training, and while the initial weights loaded into the network provided a good starting point, without overfitting prevention methods, the validation accuracy was unstable and it did not increase, showing the models inability to generalize the information acquired during training.

Figure 4.2 shows the training evolution of the same network with overfitting prevention methods used, namely the use of dropout. As is evidenced by 4.2(a), in this case, while not exactly converging, the training loss and the validation loss do not diverge as the network is trained, which evidences the effectiveness of the dropout method to prevent overfiting. In figure 4.2(b), the evolution of the accuracy in each epoch is evidenced, showing a stabilization of the validation around 70%.

To simulate early stopping, the best performing network was saved and then tested against a validation set that was not used during training and evaluated across 2 metrics in addition to accuracy: sensitivity and specificity which can be defined as follows:

$$Sensitivity = \frac{TP}{TP + FN} \qquad\qquad Specificity = \frac{TN}{TN + FP}$$

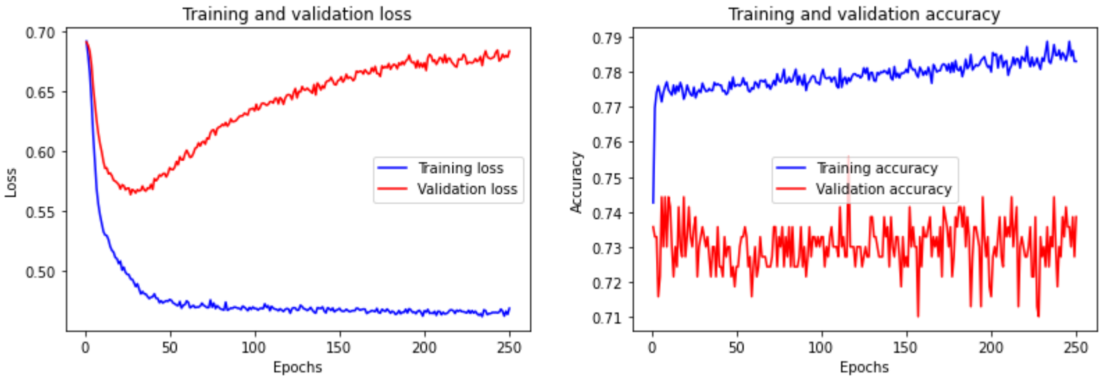

(a) Loss evolution per epoch

(b) Accuracy evolution per epoch

Figure 4.1: Training and validation metrics for ANN without dropout method. *Left:* Validation and training loss per epoch; *Right:* Validation and training accuracy per epoch.

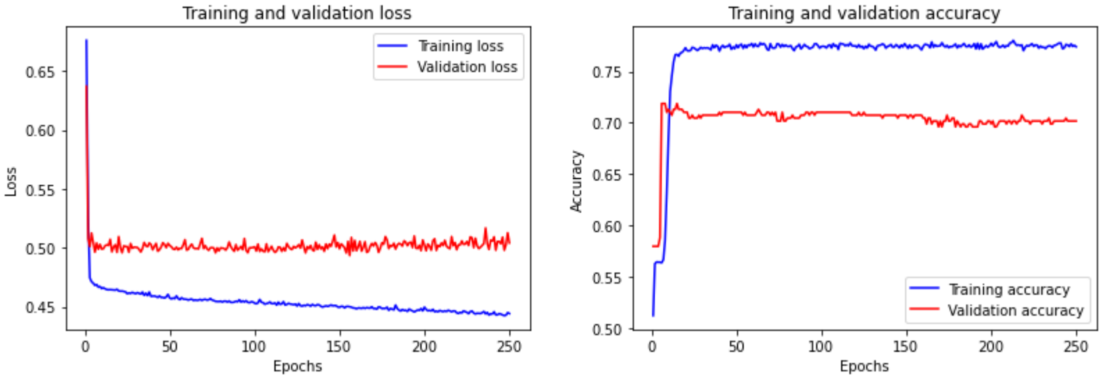

(a) Loss evolution per epoch

(b) Accuracy evolution per epoch

Figure 4.2: Training and validation metrics for ANN with dropout method. *Left:* Validation and training loss per epoch; *Right:* Validation and training accuracy per epoch.

where TP is true positives, FP is false positives, TN is true negatives and FN is false negatives.

Overall the obtained results for the final ANN were:

$Senstivity$	$Specificity$	$Accuracy$
73,13%	78,81%	76,21%

Table 4.1: ANN validation results.

While above the convergence accuracy, the validation set corresponds to only 10% of the original data set of ≈ 6000 points, which corresponds to a small amount. However, accuracy for this method remains above 70% in any test set of the original data which are promising results.

4.2 Convolutional Neural Network

On this section, the results obtained from the use of convolutional neural networks will be demonstrated.

Figure 4.3 represents the evolution of the CNN metrics during training. As shown in figure 4.3(a), the loss started reducing, however from approximately epoch 75 onwards it is clear the training is resulting in some overfitting. This is also evidenced in figure 4.3(b) where the validation accuracy starts decreasing while training accuracy evolves.

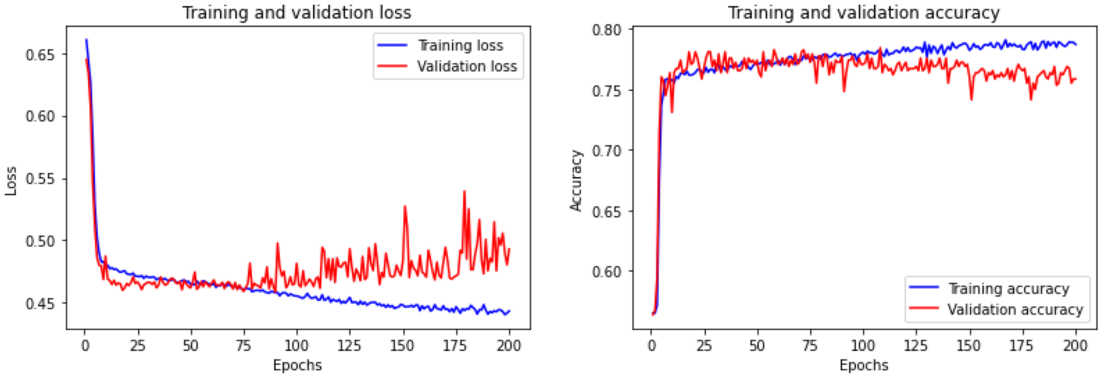

(a) Loss evolution per epoch

(b) Accuracy evolution per epoch

Figure 4.3: Training and validation metrics for CNN trained with synthetic data. *Left:* Validation and training loss per epoch; *Right:* Validation and training accuracy per epoch.

To simulate early stopping, the best performing network weights were saved and used to further fine tune the network training parameters in order to increase the accuracy. In particular, the learning rate was reduced to facilitate the convergence of the validation metrics with the training metrics. Below are the results achieved with this fine tuning:

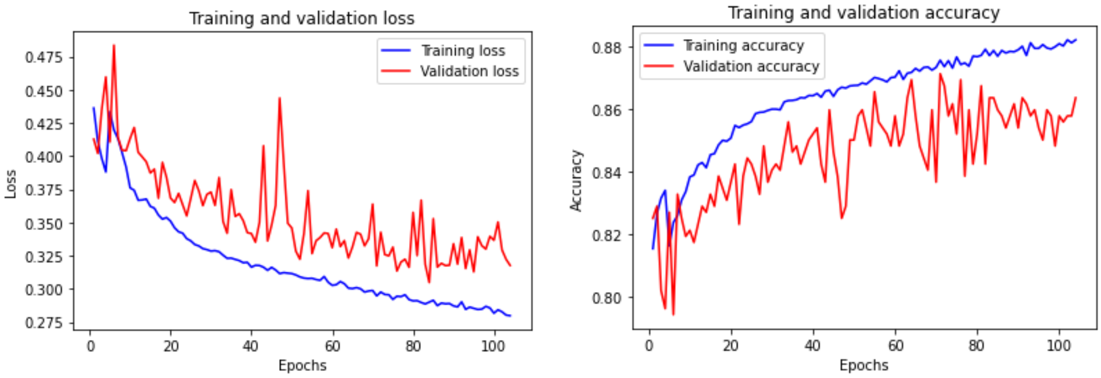

(a) Loss evolution per epoch

(b) Accuracy evolution per epoch

Figure 4.4: Training and validation metrics for CNN fin tuned with synthetic data. *Left:* Validation and training loss per epoch; *Right:* Validation and training accuracy per epoch.

As evidenced in figure 4.4, reducing the learning rate helped improve the CNN accuracy and reduce its loss while avoiding overfitting.

Once again, the weights of the best performing CNN were used to assess the network performance across the same metrics as the ANN. Below are the results:

$Senstivity$	$Specificity$	$Accuracy$
78,31%	90,88%	86,93%

Table 4.2: CNN validation results.

As stated in section 3.3.2, the VGG network was used as a benchmark for the CNN performance and was trained on the same data set with the same data augmentation conditions of the designed CNN. Table 4.3 presents the results obtained with the best performing network obtained with this architecture:

$Senstivity$	$Specificity$	$Accuracy$
98,23%	73,17%	82,95 %

Table 4.3: VGG validation results.

Chapter 5

Conclusions

The following section will present the achievements of this thesis and delineate a path for future work.

5.1 Achievements

Based on FM images obtained of *in vivo* cell cultures, the primary goal of this thesis was to develop a simple way of correctly identifying the cell phase of a particular cell.

Currently, FM based methods for accessing the cell status of individual cells are only capable of probing specific parts of the cell cycle, such as metabolic labeling procedures who only identify cells transversing the S-Phase [59] or staining methods who rely on specific cell markers [60], or are very laborious since they evolve the growth of cultures with phase specific identifiers, such as the FUCCI method used as validation for this work. While some of these second methods are capable of monitoring all phases in the cell cycle, they are not universal and are dependent on the cellular system chosen. This approach results in a very complex process which requires the use of multiple imaging channels and inhibit the capability to visualize other cell features in the same culture.

By contrast, the method suggested in this thesis relies on the use of a inexpensive and commonly used compound, the DNA dying die DAPI. This compound, allows the extraction of information from fluorescence imaging thanks to the image processing pipeline explained in section 3. Particularly, it allows the extraction of information representing both the nucleus area and the amount of DNA, two intrinsic features who provide a good description of the cell status along its cellular cycle.

While some other machine learning methods rely on the information gathered from the DAPI stain have already been proposed [43] with good results (accuracy $> 95\%$), they relied on the use of clustering algorithms which require the use of information gathered from an entire cell culture and are not capable of identifying a single data point. The method proposed for this thesis implemented the use of deep learning techniques, that were capable, after proper training, of identifying the cell phase from a single data point, not requiring information from entire cell cultures after the training phase was completed. To achieve this goal, both an ANN and a CNN were used to analyze and classify the data set obtained from the FUCCI stained cell cultures.

The ANN method relied on the manual extraction of the intrinsic features of the nucleus, area and intensity, that should translate adequately the cell phase of a single nucleus. By using this method an accuracy of $\approx 76\%$ was obtained when classifying cells in either the G1 or the S/G2/M phase. A result which, while lower than the accuracy obtained in clustering methods, it still demonstrates a clear correlation between the selected features and the cell phase. One possible explanation for this difference in accuracy is potentially the data normalization technique used. Combining the fluorescence images from various cultures, which were obtained at different times from cultures that could have reacted differently to the staining procedure, was essential to uniformize the data set. However, as a result of this normalization it is possible that some data points might have lost their correlation between their features and their label.

In addition to the ANN method, two CNNs were also used in this thesis in conjunction with data augmentation techniques. The first network was a self designed simple CNN with only two convulational layers which produced an accuracy of $\approx 87\%$ while the second network used was resorted to the architecture of a VGG network which produced an accuracy of $\approx 83\%$. Both of these networks did not rely on the manual extraction of features, rather relying on the automatic identification of features that translated the cell phase. While the results achieved are still below the ones obtained with clustering algorithms, the increase in accuracy compared with the ANN still demonstrates that the use of a CNN to address image based cell classification is a promising solution. Particularly, the further fine tune of the VGG network used could result in accuracy results comparable to the one's achieved with clustering methods, since limited fine tuning was performed in this network due to its heavy computational requirements to train which limited its development during this work.

While below the results accomplished with clustering methods, the results achieved with the methods proposed were very satisfactory and represent a promising solution to the problem of image based cell classification for a single nucleus.

5.2 Future Work

As previously stated, the use of deep learning techniques resulted in promising results to analyze and classify the cell phase through the use of fluorescence images. Particularly, the use of CNNs has shown potential as a solution for this problem.

As such, a more complex CNN should be used and fine-tuned with a larger dataset than the one currently available to try and improve the results obtained during this work.

Additionally, a multi class classification should be tried instead of the current binary one to distinguish between the different phases in the current class of the G2/S/M. However, to implement this classifier in a supervised learning method as the ones used here, other biological imaging techniques would be required to produce the validation information for the data set.

Bibliography

[1] M. Malumbres and M. Barbacid. Cell cycle, cdks and cancer: a changing paradigm. *Nature Reviews Cancer*, 9:153–166, 2009.

[2] D. Hanahan and R. A. Weinberg. Hallmarks of cancer: The next generation. *Cell*, 144(5):646 – 674, 2011.

[3] D. Jackson and P. R. Cook. Analyzing dna replication i: Labeling animals, tissues, and cells with bromodeoxyuridine (brdu). *Cold Spring Harbor Protocols*, 2008(8):pdb.prot5031, 2008.

[4] M. Hesse, A. Raulf, G.-A. Pilz, C. Haberlandt, A. M. Klein, R. Jabs, H. Zaehres, C. J. Fügemann, K. Zimmermann, J. Trebicka, A. Welz, A. Pfeifer, W. Röll, M. I. Kotlikoff, C. Steinhäuser, M. Götz, H. R. Schöler, and B. K. Fleischmann. Direct visualization of cell division using high-resolution imaging of m-phase of the cell cycle. *Nature Communications*, 3:1076, 2012.

[5] G. V.-T. C. M. T. Roukos, Vassilisand Pegoraro. Cell cycle staging of individual cells by fluorescence microscopy. 10:334–348, 2015.

[6] Y. Nagao, M. Sakamoto, T. Chinen, Y. Okada, and D. Takao. Robust classification of cell cycle phase and biological feature extraction by image-based deep learning. *Molecular Biology of the Cell*, pages mbc–E20, 2020.

[7] C. L. Chen, A. Mahjoubfar, L.-C. Tai, I. K. Blaby, A. Huang, K. R. Niazi, and B. Jalali. Deep learning in label-free cell classification. *Scientific reports*, 6:21471, 2016.

[8] C. M. O'Connor and J. U. Adams. *Essentials of Cell Biology*. NPG Education, 2010.

[9] B. Editors. Eukaryotic cell. https://biologydictionary.net/eukaryotic-cell/.

[10] C. M. O'Connor and J. U. Adams. *Essentials of Cell Biology*. NPG Education, 2010.

[11] Chapter 40 - introduction to the cell cycle. In T. D. Pollard, W. C. Earnshaw, J. Lippincott-Schwartz, and G. T. Johnson, editors, *Cell Biology (Third Edition)*, pages 697 – 711. Elsevier, third edition edition, 2017. ISBN 978-0-323-34126-4. doi: https://doi.org/10.1016/B978-0-323-34126-4.00040-2. URL `http://www.sciencedirect.com/science/article/pii/B9780323341264000402`.

[12] A. Carnero. Targeting the cell cycle for cancer therapy. *British Journal of Cancer*, 87:129–133, 2002.

[13] H. Kreipe and R. Parwaresch. A closer look at the cell cycle. *Virchoes Archives*, 422:341–343, 1993.

[14] M. C. Genome. Cell cycle control. https://www.mycancergenome.org/content/pathways/cell-cycle-control/.

[15] M. Tessema, U. Lehmann, and H. Kreipe. Cell cycle and no end. *Virchows Archive*, 444(4):313–323, 2004.

[16] J. Blow. *Replication Licensing System*, pages 3258–3262. Springer Berlin Heidelberg, Berlin, Heidelberg, 2011. ISBN 978-3-642-16483-5. doi: 10.1007/978-3-642-16483-5_5037. URL `https://doi.org/10.1007/978-3-642-16483-5_5037`.

[17] M. Schwab. *Encyclopedia of Cancer*. Springer, 2009.

[18] C. M. O'Connor and J. U. Adams. *Essentials of Cell Biology*. NPG Education, 2010.

[19] U. of Leicester. The cell cycle, mitosis and meiosis. https://www2.le.ac.uk/projects/vgec/highereducation/topics/cellc mitosis-meiosis.

[20] X. Graña and E. P. Reddy. Cell cycle control in mammalian cells: role of cyclins, cyclin dependent kinases (cdks) growth supressor genes and cyclin-dependent kinase inhibitors (ckis). *Oncogene*, 11:211–219, 1995.

[21] Z. T. irak. Investigation of tadf properties of novel donor-acceptor type pyrazine derivatives. *Journal of the Chilean Chemical Society*, 64:4303 – 4309, 03 2019. ISSN 0717-9707.

[22] J. W. Lichtman and J.-A. Conchello. Fluorescence microscopy. *Nature Methods*, 2(12):910–919, 2005.

[23] B. I. Tarnowski, F. G. Spinale, and J. H. Nicholson. Dapi as a useful stain for nuclear quantitation. *Biotechnic & Histochemistry*, 66(6):296–302, 1991.

[24] S. Hamada and S. Fujita. Dapi staining improved for quantitative cytofluorometry. *Histochemistry*, 79(2):219–226, 1983.

[25] A. Sakaue-Sawano, H. Kurokawa, T. Morimura, A. Hanyu, H. Hama, H. Osawa, S. Kashiwagi, K. Fukami, T. Miyata, H. Miyoshi, T. Imamura, M. Ogawa, H. Masai, and A. Miyawaki. Visualizing spatiotemporal dynamics of multicellular cell-cycle progression. *Cell*, 132(3):487 – 498, 2008.

[26] Fluorescent cellular changes associated with fucci cell cycle sensor, . https://www.moleculardevices.com/en/assets/app-note/dd/img/evaluating-cell-cycle-inhibitors-using-live-cell-assaygref.

[27] C. M. Bishop. *Pattern Recognition and Machine Learning (Information Science and Statistics)*, chapter 1, pages 1–12. Springer-Verlag, 2006.

[28] S. Russell and P. Norvig. *Artificial Intelligence: A Modern Approach*, chapter 18, pages 693–757. Series in Artificial Intelligence. Prentice Hall, 3 edition, 2010.

[29] Y. LeCun. The power and limits of deep learning: In his iri medal address, yann lecun maps the development of machine learning techniques and suggests what the future may hold. *Research-Technology Management*, 61(6):22–27, 2018.

[30] Y. LeCun, Y. Bengio, and G. Hinton. Deep learning. *Nature*, 521:436–444, 2015.

[31] C. M. Bishop. *Pattern Recognition and Machine Learning (Information Science and Statistics)*, chapter 5, pages 225–284. Springer-Verlag, 2006.

[32] A review of the math used in training a neural network, . https://morioh.com/p/d70aa769173a.

[33] I. Goodfellow, Y. Bengio, and A. Courville. *Deep Learning*, chapter 6, pages 168–227. The MIT Press, 2016.

[34] F. Bre, J. Gimenez, and V. Fachinotti. Prediction of wind pressure coefficients on building surfaces using artificial neural networks. *Energy and Buildings*, 158, 11 2017.

[35] S. B. Kotsiantis, I. Zaharakis, and P. Pintelas. Supervised machine learning: A review of classification techniques. *Emerging artificial intelligence applications in computer engineering*, 160:3–24, 2007.

[36] A. Abraham. *Handbook of Measuring System Design*, chapter Artificial Neural Networks. John Wiley & Sons, Ltd., 2005.

[37] M. Gardner and S. Dorling. Artificial neural networks (the multilayer perceptron)—a review of applications in the atmospheric sciences. *Atmospheric Environment*, 32(14):2627 – 2636, 1998.

[38] I. Goodfellow, Y. Bengio, and A. Courville. *Deep Learning*, chapter 9, pages 330–372. The MIT Press, 2016.

[39] C. M. Bishop. *Pattern Recognition and Machine Learning (Information Science and Statistics)*, chapter 5.5.6, pages 267–269. Springer-Verlag, 2006.

[40] Convolution-definition. `http://mathworld.wolfram.com/Convolution.html`. Accessed: 20-11-2018.

[41] A. Krizhevsky, I. Sutskever, and G. E. Hinton. Imagenet classification with deep convolutional neural networks. In F. Pereira, C. J. C. Burges, L. Bottou, and K. Q. Weinberger, editors, *Advances in Neural Information Processing Systems 25*, pages 1097–1105. Curran Associates, Inc., 2012.

[42] A. Sakaue-Sawano, H. Kurokawa, T. Morimura, A. Hanyu, H. Hama, H. Osawa, S. Kashiwagi, K. Fukami, T. Miyata, H. Miyoshi, T. Imamura, M. Ogawa, H. Masai, and A. Miyawaki. Visualizing spatiotemporal dynamics of multicellular cell-cycle progression. *Cell*, 132(3):487 – 498, 2008. ISSN 0092-8674. doi: https://doi.org/10.1016/j.cell.2007.12.033. URL `http://www.sciencedirect.com/science/article/pii/S0092867408000548`.

[43] I. Sahumbaiev. Cell cycle staging from dapi and fluorescence microscopy. Master's thesis, Instituto Superior Técnico, 2015.

[44] M. Bertero and P. Boccacci. *Introduction to inverse problems in imaging*. CRC press, 1998.

[45] I. C. Rodrigues and J. M. R. Sanches. Convex total variation denoising of poisson fluorescence confocal images with anisotropic filtering. *IEEE Transactions on Image Processing*, 20(1):146–160, 2011.

[46] M. Y. P. Maria M. Suarez-Alvarez, Duc-Truong Pham and Y. I. Prostov. Statistical approach to normalization of feature vectors and clustering of mixed datasets. *The Royal Society*, 2012.

[47] G. Gan, C. Ma, and J. Wu. *Data clustering: theory, algorithms, and applications*. SIAM, 2007.

[48] G. W. Milligan and M. C. Cooper. A study of standardization of variables in cluster analysis. *Journal of classification*, 5(2):181–204, 1988.

[49] N. Srivastava, G. Hinton, A. Krizhevsky, I. Sutskever, and R. Salakhutdinov. Dropout: a simple way to prevent neural networks from overfitting. *The journal of machine learning research*, 15(1): 1929–1958, 2014.

[50] S. Khirirat, H. R. Feyzmahdavian, and M. Johansson. Mini-batch gradient descent: Faster convergence under data sparsity. In *2017 IEEE 56th Annual Conference on Decision and Control (CDC)*, pages 2880–2887, 2017.

[51] I. Goodfellow, Y. Bengio, and A. Courville. *Deep Learning*, chapter 1, pages 1–28. The MIT Press, 2016.

[52] C. Shorten and T. M. Khoshgoftaar. A survey on image data augmentation for deep learning. *Journal of Big Data*, 6(1):60, Jul 2019.

[53] L. Prechelt. Early stopping-but when? In *Neural Networks: Tricks of the trade*, pages 55–69. Springer, 1998.

[54] L. Deng. The mnist database of handwritten digit images for machine learning research [best of the web]. *IEEE Signal Processing Magazine*, 29(6):141–142, 2012.

[55] Mnist reborn, restored and expanded: Additional 50k training samples, . https://medium.com/syncedreview/mnist-reborn-restored-and-expanded-additional-50k-training-samples-70c6f8a9e9a9.

[56] K. Simonyan and A. Zisserman. Very deep convolutional networks for large-scale image recognition. *arXiv preprint arXiv:1409.1556*, 2014.

[57] A. Krizhevsky, I. Sutskever, and G. E. Hinton. Imagenet classification with deep convolutional neural networks. In *Advances in neural information processing systems*, pages 1097–1105, 2012.

[58] Vgg16 – convolutional network for classification and detection, . https://neurohive.io/en/popular-networks/vgg16/.

[59] D. Jackson and P. R. Cook. Analyzing dna replication i: labeling animals, tissues, and cells with bromodeoxyuridine (brdu). *Cold Spring Harbor Protocols*, 2008(8):pdb–prot5031, 2008.

[60] H. Leonhardt, H.-P. Rahn, P. Weinzierl, A. Sporbert, T. Cremer, D. Zink, and M. C. Cardoso. Dynamics of dna replication factories in living cells. *The Journal of cell biology*, 149(2):271–280, 2000.